Phys Chem Minerals (2004) 31: 299 – 305
DOI 10.1007/s00269-004-0391-1

ORIGINAL PAPER

J. Zhao · N. L. Ross · R. J. Angel

Tilting and distortion of $CaSnO_3$ perovskite to 7 GPa determined from single-crystal X-ray diffraction

Received: 25 August 2003 / Accepted: 11 February 2004

Abstract The structural changes of $CaSnO_3$, a $GdFeO_3$-type perovskite, have been investigated to 7 GPa in a diamond-anvil cell at room temperature using single-crystal X-ray diffraction. Significant changes are observed in both the octahedral Sn–O bond lengths and tilt angles between the SnO6 octahedra. The octahedral (SnO6) site shows anisotropic compression and consequently the distortion of SnO6 increases with pressure. Increased pressure also results in a decrease of both of the inter-octahedral angles, ∠Sn–O1–Sn and ∠Sn–O2–Sn, indicating that octahedral tilting increases with increasing pressure, chiefly equivalent to rotation of the SnO6 octahedra about the pseudocubic $< 001 >_p$ axis. The distortion in the CaO12 and SnO6 sites, along with the octahedral SnO6 tilting, is attributed to the SnO6 site being less compressible than the CaO12 site.

Keywords Perovskite · X-ray diffraction · Crystal structure · High pressure

Introduction

The $GdFeO_3$-type perovskites, with general stoichiometry ABO_3, are framework structures of corner-linked BO6 octahedra that display orthorhombic symmetry (P*bnm*) and are derived from the ideal cubic structure (*Pm*3*m*) via the tilting and distortion of BO6 octahedra (Glazer 1972; Woodward 1997a,b). The $CaBO_3$ perovskites (B = Zr, Sn, Ti, and Ge) are $GdFeO_3$-type perovskites with distortions different from the ideal cubic structure. One measure of the distortion is reflected in the tilt angles between the octahedra, B–O1–B and B–O2–B, which are both 180° in the cubic prototype. $CaSnO_3$ and $CaZrO_3$ have average B–O–B tilt angles of 147° and 146°, respectively, compared with $CaTiO_3$ and $CaGeO_3$ which have average tilt angles of 156° and 160°, respectively. Previous studies have shown that the isothermal bulk moduli (K_{T0}) of these Ca-oxide perovskites fall on a single smooth trend with inverse molar volume, V_m (Ross and Chaplin 2003). At larger unit-cell volumes (i.e. lower atomic packing densities) the bulk modulus is smaller and the perovskites are softer. In simple oxide structures in which no phase transitions occur, the relationship between bulk moduli and specific volume is often linear, i.e. $K_{T0}V_m = \text{constant}$ (Anderson and Anderson 1970). However, the trend of K_{T0} with $1/V_m$ of the Ca-oxide perovskites displays significant curvature in large part due to K_{T0} of $CaSnO_3$, 162.6 ± 1.0 GPa (Kung et al. 2001), that is greater than that predicted by a linear trend. The compression mechanism responsible for this anomalous stiffening of $CaSnO_3$ is unknown.

Hazen and Finger (1982) developed the general ideal that bulk compressibility of most metal oxides is closely related to polyhedral compression and polyhedral linkage. For a framework structure with corner-linked polyhedra, compression is generally achieved through tilting of polyhedra which act as rigid units (Hazen and Finger 1982). This theory has been further developed within the context of the rigid-unit model and has been successfully applied to many tetrahedral framework structures (e.g. Dove et al. 1995; Dove 1997;Hammonds et al. 1998). However, the treatment of polyhedra as rigid units neglects changes in their distortion that may or may not occur at high pressure. In $GdFeO_3$-type perovskites, accumulated evidence suggests that the relative compressibilities of the AO12 and BO6 sites play an important role in the evolution of distortion and tilting of BO6 under high pressure (O'Keeffe et al. 1979; Andrault and Poirier 1991; Ross 1996, 1998; Ross and Hazen 1990). However, in order to understand the compression mechanisms in $GdFeO_3$-type perovskites, it is necessary to carry out accurate atomic-level

J. Zhao · N. L. Ross (✉) · R. J. Angel
Department of GeoSciences,
Virginia Polytechnic Institute and State University,
Blacksburg, VA 24061, USA
E-mail: nross@vt.edu
Fax: 540-231-3386

measurements of high-pressure structural parameters, which enables one to examine in detail the compressibilities of individual bonds within both BO6 and AO12 sites, and tilting between BO6 octahedra. Such a study requires high-quality structure refinements from high-quality single crystals loaded in diamond-anvil cells. However, determination of high-pressure structural parameters obtained from single-crystal X-ray diffraction measurements is hampered by uncertainties due to lack of access to reflections in the DAC combined with absorption and diffraction by the components of the DAC (e.g. Angel et al. 2000, 2003). It therefore becomes challenging to measure the subtle variation of individual B–O and A–O bond lengths and angles in the perovskite structure at high pressure. Recently, several improvements have been made to reduce these uncertainties in high-pressure single-crystal X-ray diffraction studies and refinements from high-pressure data are now approaching those obtained from crystals in air (Angel et al. 2003). Thus it becomes feasible to derive the insights into the evolution of distortion and tilting of ''rigid polyhedra'' in relatively stiff materials like $CaSnO_3$

We have therefore undertaken a high-pressure single-crystal X-ray diffraction study of $CaSnO_3$ perovskite to determine the compression mechanism(s) operative in $CaSnO_3$ at high pressure and to determine whether the approximation of octahedra as ''rigid units'' is valid for distorted *Pbnm* perovskites. These results have wider implications for studies of other *Pbnm* perovskites at high pressure, such as $MgSiO_3$ perovskite, which is believed to be the dominant phase in the Earth's lower mantle (e.g. Navrotsky and Weidner 1989).

Experimental

The single crystal of $CaSnO_3$ was selected from the same batch of crystals synthesized in an earlier study (Kung et al. 2001). The synthesis involved heating a 2:1 (molar) mixture of $CaCl_2$ and SnO_2 to 1200 °C for 24 h, cooling the reactant from the melt to room temperature, and separating the residual chlorides from solid reactant in distilled water (Vegas et al. 1986). A single-crystal $CaSnO_3$ with pseudocubic habit (120 × 120 × 100 μm) was selected for high-pressure measurement after X-ray diffraction measurements in air that confirmed that there was no twinning. The crystal was oriented with a face parallel to (110) and polished to ~60 μm thickness in order to gain access to the maximum number of reflections along the three crystallographic axes.

The crystal was loaded with (110) parallel to the surface of a 600-μm anvil of an ETH diamond anvil cell (Miletich et al. 2000). A 200-μm-thick T301 steel gasket was preindented to a thickness of 110 μm and a hole of $\phi = 280$ μm was drilled in the centre of the indented region. A ruby sphere (~10 μm in diameter) was also loaded into the cavity to serve as a pressure calibrant (Mao et al. 1986). The shift of R-luminescence lines was measured by using a Dilor XY 0.64 meter Raman microprobe and accessory spectrometer with CCD multichannel detector. Errors of pressures were estimated from two measurements before and after data collections. A 4:1 methanol:ethanol mixture served as the pressure-transmitting medium.

Intensity data for all accessible reflections were collected at room pressure (in the DAC) and at 0.738, 1.50, 2.61, 3.94, 5.18, 5.98 and 6.73 GPa. Unit-cell parameters at three pressure points were measured on a Huber four-circle diffractometer (Mo Kα 50 kV, 40 mA) using the eight-position-centring technique (King and Finger 1979) and the other five sets of unit-cell parameters were determined from the equation of state of $CaSnO_3$ obtained by using the same technique (Kung et al. 2001). The intensity data were collected by using ω scans with the fixed-ϕ mode (Finger and King 1978) from 2° to 40° in θ on an Xcalibur diffractometer (Mo Kα, 50 kV, 40 mA). We determined the offset of the crystal from the rotation axis of the goniometer by measuring between 20 to 40 strong low-angle reflections and calculating the crystal offsets from the reflection positions with the WinIntegrStp program, v3.3 (Angel 2003). We found that it was critical to eliminate these offsets by adjusting the DAC on the goniometer before data collection. Peak fitting and integration of intensities were carried out by using the WinIntegrStp 3.3 software. Other corrections such as absorption effects of DAC, including correction of beryllium plates, diamond anvils, shadowing by the gasket and the sample itself, were made by using ABSORB 5.3 (Angel 2003b) which is based on Burnham's (1966) methods and original code. After the crystallographically equivalent reflections were averaged, the remaining independent reflections with ($F > 4\sigma(F)$) were applied to refine structures with RFINE99, a development version RFINE4 (Finger and Prince 1975). The number of reflections increases with pressure because the gasket becomes thinner and the shadowing effect of the gasket is reduced. Details of all refinement information, the

Table 1 Refinement information for $CaSnO_3$ perovskite at high pressures

P, GPa:	0.0	0.738(16)	1.50(5)	2.61(2)	3.94(1)	5.18(3)	5.98(6)	6.73(9)
N [$> 2\ I_0/\sigma(I_0)$][a]	781	778	763	747	729	724	721	726
N [$F > 4\sigma(F)$][b]	223	230	248	266	277	262	282	270
R_{int}(N)[c]	0.0155 (215)	0.0173 (216)	0.0168 (230)	0.0176 (231)	0.0162 (233)	0.0196 (234)	0.0186 (239)	0.0189 (235)
G_{fit}[d]	1.08	1.14	1.18	1.15	1.25	1.07	1.17	0.99
Extinction Factor($\times 10^{-4}$)	0.11(6)	0.11(6)	0.11(6)	0.10(5)	0.10(5)	0.93(5)	0.75(5)	0.94(5)
R_w[e]	0.022	0.026	0.026	0.024	0.027	0.024	0.025	0.027
R_{uw}[f]	0.018	0.020	0.020	0.021	0.022	0.024	0.025	0.022

[a] Number of reflections with $I > 2\ I_0\ /\ \sigma(\ I_0)$
[b] R_{int}, number of independent reflections with $F > 4\sigma(F)$
[c] Internal residual on F (number of averaged reflections)
[d] Estimated standard deviation of unit weight observation
[e] Weighted $R_w = [\Sigma w(|F_0|\text{-}|F_c|)^2/\Sigma|F_0|^2]^2$
[f] Unweighted $R_{uw} = \Sigma||F_0|\text{-}|F_c||/\Sigma|F_0|$
[g] A weight of $1/\sigma_F{}^2$ assigned to each reflection, where σ_F is based on counting statistics

Table 2 Unit-cell parameters, refined positional parameters and anistropic temperature factors (β_{ij}) and equivalent isotopic temperatures factors (B_{eq}) of $CaSnO_3$ perovskite at high pressure

P, (GPa)	0.0	0.738(16)	1.50(5)	2.61(2)	3.94(1)	5.18(3)	5.98(6)	6.73(9)
a (Å)	5.5142(2)	5.5043(2)	5.4952(6)	5.4824(2)	5.4676(1)	5.4538(3)	5.44480(14)	5.43626(18)
b (Å)	5.6634(2)	5.6558(2)	5.6486(4)	5.6384(2)	5.6267(1)	5.6162(2)	5.60887(13)	5.60235(18)
c (Å)	7.88162(17)	7.8687(3)	7.8561(8)	7.8387(3)	7.8186(1)	7.8006(4)	7.78906(10)	7.77743(10)
Ca[a]								
x	−0.01265(16)	−0.01294(16)	−0.01276(17)	−0.01290(15)	−0.01313(16)	−0.01276(15)	−0.01314(13)	−0.01364(13)
y	0.0505(3)	0.0505(3)	0.0509(3)	0.0515(3)	0.0517(3)	0.0520(3)	0.0528(3)	0.0528(3)
*B*eq	0.564(17)	0.558(18)	0.556(19)	0.525(17)	0.531(18)	0.514(15)	0.545(16)	0.489(17)
β11	0.0034 (5)	0.0045(5)	0.0046(5)	0.0043(5)	0.0041(5)	0.0043(4)	0.0046(4)	0.0039(4)
β22	0.0053 (5)	0.0041(5)	0.0042(5)	0.0040(5)	0.0044(5)	0.0041(4)	0.0039(4)	0.0043(5)
β33	0.00237(11)	0.00246(12)	0.00235(11)	0.00227(10)	0.00223(10)	0.00209(9)	0.00249(10)	0.00194(9)
β12	−0.00062(18)	−0.00052(19)	0.00002(22)	0.00029(16)	−0.00036(21)	−0.00102(18)	−0.00090(16)	−0.00064(15)
Sn[b]								
*B*eq	0.305(13)	0.298(14)	0.305(13)	0.287(12)	0.279(13)	0.272(12)	0.292(12)	0.290(14)
β11	0.0021(3)	0.0020(3)	0.00242(28)	0.00238(26)	0.00248(26)	0.00275(24)	0.00267(23)	0.00267(26)
β22	0.0030(3)	0.0020(3)	0.00285(25)	0.00259(25)	0.00236(25)	0.00189(23)	0.00223(26)	0.00242(28)
β33	0.00108(6)	0.00111(6)	0.00105(6)	0.00099(6)	0.00099(6)	0.00102(5)	0.00116(5)	0.00104(6)
β12	0.00001(4)	0.00005(3)	−0.00001(4)	0.00003(4)	0.00004(4)	0.00001(3)	0.00000(3)	0.00005(3)
β13	0.00002(4)	−0.00001(4)	−0.00002(4)	0.00001(4)	0.00001(4)	−0.00004(4)	0.00005(3)	0.00014(3)
β23	0.00008(3)	0.00002(3)	0.00010(3)	0.00005(4)	0.00008(3)	0.00003(3)	0.00002(3)	0.00001(3)
O1[c]								
x	0.0993(8)	0.1009(8)	0.1009(9)	0.1004(7)	0.1014(7)	0.1006(7)	0.1019(6)	0.1023(6)
y	0.4646(6)	0.4648(7)	0.4637(8)	0.4633(6)	0.4651(5)	0.4643(5)	0.4634(6)	0.4647(5)
*B*eq	0.60(5)	0.58(5)	0.63(6)	0.49(5)	0.39(5)	0.49(5)	0.53(5)	0.48(5)
β11	0.0058(20)	0.0096(21)	0.0062(21)	0.0062(17)	0.0027(18)	0.0068(17)	0.0057(14)	0.0073(17)
β22	0.0068(18)	0.0026(19)	0.0062(21)	0.0044(16)	0.0056(17)	0.0025(16)	0.0049(15)	0.0032(15)
β33	0.0010(3)	0.0010(3)	0.0014(3)	0.0006(4)	0.0006(3)	0.0015(4)	0.0013(3)	0.0007(3)
β12	−0.0005(8)	−0.0005(7)	0.0010(8)	0.0003(7)	−0.0003(8)	−0.0010(6)	−0.0012(6)	−0.0006(6)
O2								
x	0.6987(4)	0.6981(4)	0.6970(4)	0.6977(4)	0.6967(4)	0.6957(4)	0.6958(3)	0.6961(4)
y	0.2988(4)	0.2981(4)	0.2995(5)	0.2983(4)	0.2996(4)	0.3007(4)	0.2993(4)	0.2989(4)
z	0.0520(3)	0.0518(3)	0.0514(3)	0.0526(3)	0.0520(3)	0.0524(2)	0.0533(2)	0.0526(2)
B_{eq}	0.56(4)	0.59(4)	0.59(4)	0.57(3)	0.51(4)	0.45(3)	0.54(3)	0.51(4)
β11	0.0034(12)	0.0008(12)	0.0010(12)	0.0050(10)	0.0040(11)	0.0034(10)	0.0045(8)	0.0034(10)
β22	0.0038(13)	0.0078(12)	0.0062(13)	0.0034(9)	0.0033(10)	0.0015(11)	0.0028(9)	0.0034(09)
β33	0.0032(3)	0.0027(2)	0.0035(3)	0.0026(2)	0.0026(2)	0.0031(3)	0.0030(2)	0.0029(2)
β12	−0.0026(5)	−0.0021(5)	−0.0016(6)	−0.0020(5)	−0.0013(5)	−0.0011(5)	−0.0014(5)	−0.0016(4)
β13	0.0011(3)	0.0011(3)	0.0007(4)	0.0001(4)	0.0005(3)	0.0005(3)	0.0003(3)	0.0003(3)
β23	−0.0016(4)	−0.0010(3)	−0.0006(4)	−0.0007(3)	−0.0002(3)	−0.0003(4)	−0.0010(3)	−0.0003(4)

[a] Ca: $z = 0.25$; $\beta13 = \beta23 = 0$
[b] Sn: $x = 0.0$, $y = 0.5$, $z = 0.5$
[c] O1: $z = 0.25$; $\beta13 = \beta23 = 0$

refined positions of atoms and thermal parameters and distances and angles are list in Tables 1, 2 and 3, respectively.

Results and discussion

Distortion of octahedral SnO6 site and the dodecahedral CaO12 site

The variation of the Sn–O bond distances as a function of pressure is shown in Fig. 1. The slopes of the individual bond lengths $Rij(P)$ ($i = Sn, j = O$) and their mean linear compressibilities are listed in Table 4. The mean linear compressibility β_{ij} of a bond is calculated using the relation, $-[1/R_{ij}(0)]\Delta R_{ij}/\Delta P$. We find that Sn–O1 and Sn–O21 have similar compressibilities, but Sn–O22 is less compressible. The individual Sn–O bond lengths decrease by 0.015, 0.024 and 0.030 Å between room pressure and 7 GPa, with individual determinations of bond distances having esd's of 0.002 Å. This result clearly shows that distortion of octahedral SnO6 increases with increasing pressure because of the different compressibilities among three bonds Sn–O1(x2), Sn–O21(x2) and Sn–O22(x2).

Figure 2a and b shows the pressure dependence of distances between Ca and its 12 nearest-neighbour oxygen atoms, with linear compressibilities given in Table 4. We notice a general trend that the longer distances are less compressible than the shorter bond distances. For example, compressibilities of the eight shortest Ca–O distances are more or less the same within the resolution of our measurements, whereas the four

Table 3 Interatomic distances (Å), angles(°) and polyhedral volumes of SnO6, V_{oct} (Å^3), and CaO12, V_{dod} (Å^3), of $CaSnO_3$ perovskite at high pressure

P (GPa):		1 bar	0.738(16)	1.50(5)	2.61(2)	3.94(1)	5.18(3)	5.98(6)	6.73(9)
Sn–O1	x2	2.0548(12)	2.0537(12)	2.0511(13)	2.0460(11)	2.0412(12)	2.0357(10)	2.0331(11)	2.0319(10)
Sn–O21	x2	2.0568(19)	2.0491(20)	2.0485(24)	2.0428(17)	2.0405(20)	2.0405(19)	2.0359(22)	2.0269(18)
Sn–O22	x2	2.0555(19)	2.0568(20)	2.0540(23)	2.0518(19)	2.0463(20)	2.0408(19)	2.0410(20)	2.0410(18)
V_{oct}		11.576(28)	11.530(29)	11.495(34)	11.420(27)	11.354(29)	11.299(27)	11.258(26)	11.198(25)
O1–Sn–O2	x2	88.30(13)	88.55(12)	88.61(15)	88.22(11)	88.67(12)	88.50(11)	88.36(11)	88.63(11)
O1–Sn–O2	x2	88.21(11)	88.11(12)	87.90(14)	88.12(11)	88.17(11)	88.26(10)	88.39(11)	88.21(10)
O1–Sn–O1	x2	180.00	180.00	180.00	180.00	180.00	180.00	180.00	180.00
O1–Sn–O2	x2	91.79(11)	91.89(12)	92.10(14)	91.88(11)	91.83(11)	91.74(10)	91.61(11)	91.79(10)
O1–Sn–O2	x2	91.70(13)	91.45(12)	91.39(14)	91.78(11)	91.33(12)	91.50(11)	91.64(11)	91.37(11)
O2–Sn–O2	x2	90.81(3)	90.72(3)	90.67(4)	90.73(3)	90.66(3)	90.68(3)	90.70(3)	90.58(3)
O2–Sn–O2	x2	89.19(3)	89.28(3)	89.33(14)	89.27(3)	89.34(3)	89.32(3)	89.30(3)	89.42(3)
O2–Sn–O2	x2	180.00	180.00	180.00	180.00	180.00	180.00	180.00	180.00
Ca–O1		2.331(3)	2.319(4)	2.316(5)	2.315(4)	2.305(5)	2.301(3)	2.299(4)	2.290(3)
Ca–O1		2.425(4)	2.426(4)	2.414(5)	2.403(3)	2.405(5)	2.399(3)	2.390(4)	2.392(4)
Ca–O1		3.271(4)	3.272(4)	3.269(5)	3.259(4)	3.253(5)	3.243(4)	3.238(4)	3.238(3)
Ca–O1		3.375(4)	3.371(4)	3.375(5)	3.375(3)	3.363(5)	3.357(3)	3.360(4)	3.354(4)
Ca–O2	x2	2.350(3)	2.347(2)	2.340(3)	2.337(2)	2.331(3)	2.317(2)	2.315(2)	2.316(2)
Ca–O2	x2	2.636(3)	2.631(3)	2.636(3)	2.617(3)	2.621(3)	2.616(2)	2.603(3)	2.598(2)
Ca–O2	x2	2.784(3)	2.779(2)	2.766(3)	2.770(2)	2.752(3)	2.747(2)	2.748(2)	2.744(2)
Ca–O2	x2	3.546(3)	3.540(3)	3.540(3)	3.536(3)	3.528(3)	3.531(2)	3.533(2)	3.521(2)
V_{dod}		49.958(24)	49.711(23)	49.469(15)	49.156(21)	48.780(26)	48.434(22)	48.210(26)	48.020(15)
Sn–O1–Sn		147.04(23)	146.61(22)	146.49(24)	146.59(21)	146.50(22)	146.66(19)	146.58(20)	146.23(18)
Sn–O2–Sn		147.87(13)	147.92(12)	147.67(13)	147.61(12)	147.43(12)	146.95(11)	147.06(10)	147.28(11)

longer Ca–O distances are significantly less compressible (Table 4). This divergence of the compressibilities within the CaO12 site results in an increase in the distortion of the dodecahedral CaO12 site.

Furthermore, the Ca site, whether considered as a CaO8 or a CaO12 polyhedron, is less compressible than SnO6. The volume of dodecahedral CaO12 was calculated by using the relation $V_{dod} = V/4\text{-}V_{oct}$, where V is unit-cell volume and V_{oct} is the volume of octahedral SnO_6 (Table 3). The polyhedral bulk moduli, K_P, and compressibilities ($\beta = 1/K_P$) were obtained by fitting the polyhedral volumes with the Birch–Murnaghan finite-strain formulism:

$$P = \frac{3}{2}K_P\left[\left(\frac{V_{0,\mathrm{poly}}}{V}\right)^{7/3} - \left(\frac{V_{0,\mathrm{poly}}}{V}\right)^{5/3}\right]\left\{1 + \frac{3}{4}(K_P' - 4)\left[\left(\frac{V_{0,\mathrm{poly}}}{V}\right)^{2/3} - 1\right]\right\}, \quad (1)$$

with the EOSFit v5.2 program (Angel 2000), where $V_{0,poly}$ is a polyhedral volume at room pressure, K_P is the polyhedral bulk modulus, and K_P' is the first derivative with respect to pressure, constrained to be 4. The polyhedral bulk moduli are 195(6) GPa and 158(2) GPa for the SnO6 site and CaO12 site, respectively. The volume compressibility of the CaO12 site ($\beta_{CaO12} = 1/K_P$), $\beta_{CaO12} = 6.33(4) \times 10^{-3}\mathrm{GPa}^{-1}$, is more than that of octahedral SnO6 site [$\beta_{SnO6} = 5.13(15) \times 10^{-3}\mathrm{GPa}^{-1}$], whereas the compressibility of unit cell [$6.15(4) \times 10^{-3}\mathrm{GPa}^{-1}$] is intermediate between them.

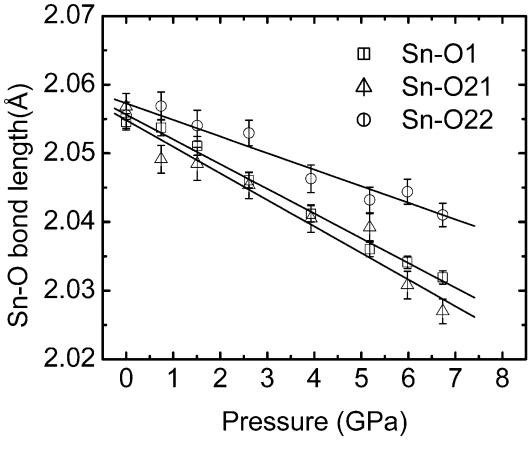

Fig. 1 The variation of the Sn–O bond distances in $CaSnO_3$ perovskite as a function of pressure

Octahedral tilting

Figure 3a shows the evolution of the inter-octahedral Sn–O1–Sn (α_1) and Sn–O2–Sn (α_2) angles with increasing pressure. Both angles show a small decrease with pressure. In addition to the Sn–O1–Sn and Sn–O2–Sn tilt angles, other angle parameters have been introduced to describe the tilting (Lelieveld and Ijdo 1980; O'Keeffe et al. 1979; Zhao et al. 1993a, b), such as (1) θ: the tilt of the octahedral about the pseudocubic $< 110 > p$ axis; (2) ϕ: the tilt of the of the octahedral about the pseudocubic $< 001 > p$ axis (Fig. 3b), which are equivalent to Φ introduced by (O'Keeffe et al. 1979). From Fig. 3b, we see that the tilting angle θ just increases within the

Table 4 Variation of Sn–O and Ca–O distances with pressure for the observed structure and "fixed atom" reference model

Interatomic distance	R_i (Å) at Room pressure	$\Delta R_{ij}/\Delta P$ Å/GPa experiment	$\Delta R_{ij}/\Delta P$ Å/GPa model	Observed linear compressibility $\beta(\times 10^{-3}\mathrm{GPa}^{-1})$	Model linear compressibility $\beta(\times 10^{-3}\mathrm{GPa}^{-1})$
Sn–O1 (x2)	2.0548(12)	−0.0036(1)	−0.00406(5)	1.75(5)	1.976(23)
Sn–O21 (x2)	2.0568(19)	−0.0039(4)	−0.00364(1)	1.90(19)	1.773(3)
Sn–O22 (x2)	2.0555(19)	−0.0024(2)	−0.00399(8)	1.17(9)	1.941(37)
Average	2.0557(2)			1.61(11)	1.90(2)
Ca–O1	2.331(4)	−0.0055(4)	−0.00472(6)	2.36(18)	2.025(22)
Ca–O1	2.425(4)	−0.0055(6)	−0.00397(8)	2.3(3)	1.637(30)
Ca–O1	3.271(4)	−0.0054(3)	−0.00680(5)	1.65(9)	2.079(12)
Ca–O1	3.375(4)	−0.0031(6)	−0.00540(6)	0.92(18)	1.600(15)
Ca–O2 (x2)	2.350(3)	−0.0058(6)	−0.00433(7)	2.5(3)	1.843(27)
Ca–O2 (x2)	2.636(3)	−0.0054(9)	−0.00493(5)	2.0(3)	1.870(17)
Ca–O2 (x2)	2.784(3)	−0.0059(7)	−0.00532(8)	2.1(3)	1.911(26)
Ca–O2 (x2)	3.546(3)	−0.0029(4)	−0.00648(18)	0.83(11)	1.827(13)
$<AO>^{vii}$	2.537			2.23	1.864(8)
$<AO>^{xii}$	2.835			1.84	1.85(2)

resolution of the measurement, whereas ϕ shows a more obvious increase with pressure. The tilting causes measurable shifts in the positions of O21 and O22, as shown in Fig. 4.

Usually, the pseudocubic unit cell is used as a reference structure model to examine the tilting and distortion of the $GdFeO_3$-type perovskite and can supply useful information about how the orthorhombic structure deviates from the cubic structure model by comparing the difference between it and the real structure. Here we introduce another reference structural model to examine the difference of the evolution structures with pressure between this reference model and real structure. We assume that the three axes a, b and c of the $CaSnO_3$ unit cell vary as the observed measured variations with increasing pressure, but the atomic coordinates (x,y,z) in the asymmetric unit do not change with pressure. This "fixed coordinate" model provides insight into how the real structure changes under pressure by showing how a "driving force" optimizes the geometric configuration of structure of model by shifting atomic coordinates or moving atoms to their equilibrium positions (real structural configuration). As we will see, this is generally equivalent to the tilting of the octahedral SnO6 with resulting distortions in the CaO12 and SnO6 sites.

As shown in Fig. 5 and in Table 4, the "fixed coordinate" model predicts that the Sn–O22 bond length becomes more compressible than the actual observed change, whereas Sn–O1 and Sn–O21 are similar to the measured ones. The mean linear compressibility of Sn–O

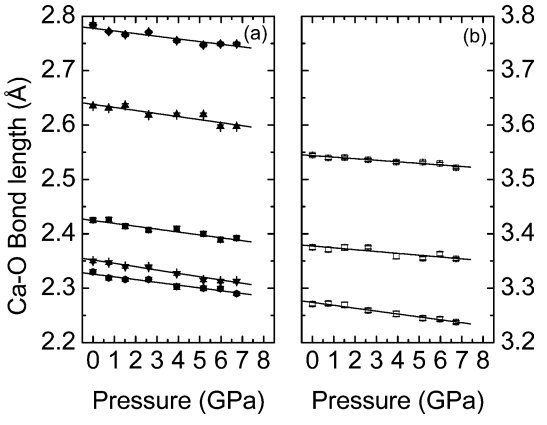

Fig. 2 **a** The variation of the eight shortest Ca–O bond lengths as a function of pressure and **b** the variation of the four longest Ca–O distances as a function of pressure

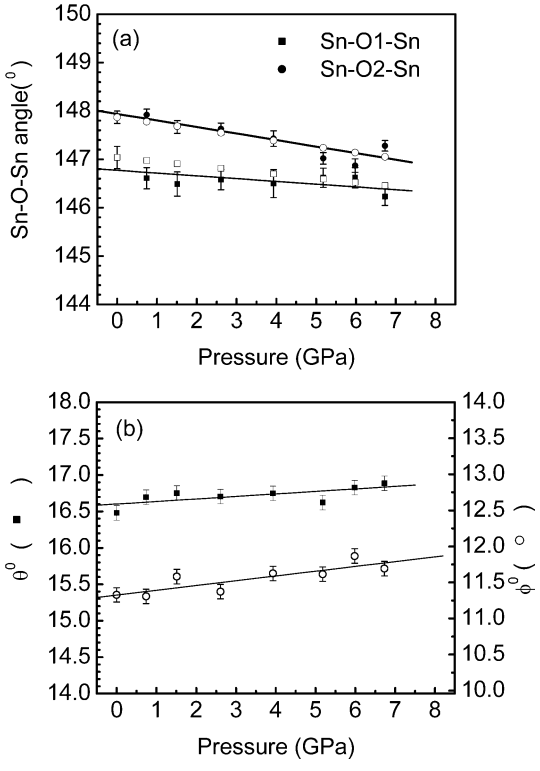

Fig. 3 **a** Pressure evolution of the octahedral tilt angles, Sn–O1–Sn and Sn–O2–Sn, of $CaSnO_3$ perovskite at high pressure (*solid symbols*), where the *hollow symbols* represent angles calculated using: $\alpha_i = 2\sin^{-1}[\exp(\Delta\beta_i P)\sin\alpha_{0i}/2]$. **b** Pressure dependence of tilting angles θ and ϕ of $CaSnO_3$

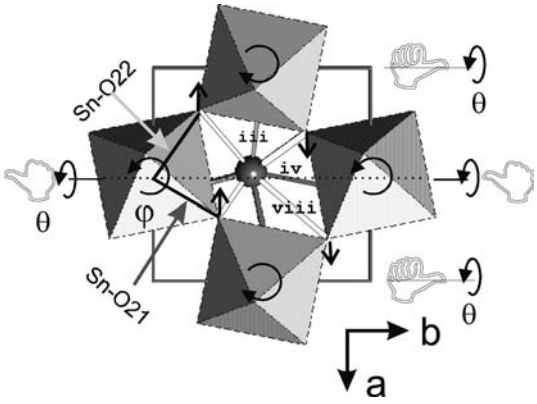

Fig. 4 Structure of $CaSnO_3$ perovskite showing the effect of pressure, including tilting of the SnO6 octahedra and displacement of O21 and O22 atoms. Ca–O2 bonds are shown in *grey* and Ca–O1 bonds are shown white. The four longer Ca–O distances (Ca–O1 *iii*, Ca–O1 *iv* and Ca–O2 *viii*) are also labelled

in the model, $1.90(2) \times 10^{-3}\text{GPa}^{-1}$, is greater than that observed, $1.61(11) \times 10^{-3}\text{GPa}^{-1}$. The eight shortest Ca–O bond lengths of the model become less compressible than the actual measured values, but the four longer Ca–O distances in the model are more compressible than those observed. This is opposite to the observed high-pressure behaviour. As a result, the model predicts that the average linear compressibility of the Sn–O bonds is greater than that of the Ca–O bonds.

The model predicts that the tilt angles between the SnO6 octahedra, Sn–O1–Sn and Sn–O2–Sn, do not change significantly with increasing pressure. For example, from room pressure to 6.7 GPa, Sn–O1–Sn and Sn–O2–Sn are predicted to vary from 147.03° to147.04° and 147.85° to 147.86°, respectively. Because Sn–O1–Sn and Sn–O2-Sn are measures of the tilting between SnO6, no octahedral tilting of SnO6 is predicted by the model. Thus, considering only axial compression of the unit cell without adjustment of atomic positional coordinates results in an incorrect model of the true structural variation of $CaSnO_3$ perovskite. A consequence of the tilting of SnO6 observed at high pressure is

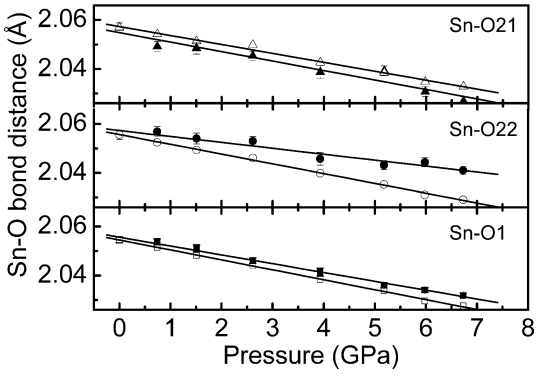

Fig. 5 Comparison of compressibility of the Sn–O bonds between the observed structure (*solid symbols*) and the "fixed-atom" reference structure (*hollow symbols*)

that the CaO12 site becomes more compressible than the SnO6 site. This is a main reason, as we will see in the following section, why the four longest Ca–O distances of the crystal are less compressible than the eight shorter Ca–O (Fig. 4).

Relationship between octahedral tilting and distortions of CaO12 and SnO6

From the geometric point of view, one of three bond lengths between three pairs of Sn–O atoms can be expressed as:

$$R_{\text{Sn–O1}} = \frac{c}{4\sin\frac{\alpha_1}{2}} \quad , \tag{2}$$

where $\alpha_1 = \angle$ Sn–O1–Sn. If one uses an average bond length $R_{\text{Sn–O2}}$ to approximate bond lengths $R_{\text{Sn–O21}}$ and $R_{\text{Sn–O22}}$, we can obtain a relation of average $R_{\text{Sn–O2}}$ to $\alpha_2 = \angle$ Sn–O2–Sn:

$$R_{\text{Sn–O2}} = \frac{\sqrt{a^2+b^2}}{4\sin\frac{\alpha_2}{2}} \quad . \tag{3}$$

From Eqs. (2) and (3), we can obtain a relation of compressibilities at room pressure between the unit-cell axes *a,b,c* and bond compressibilities as:

$$\beta_{\text{Sn–O1}} = \beta_c + \frac{1}{\sin\frac{\alpha_1}{2}}\left(\frac{d\sin\frac{\alpha_1}{2}}{dP}\right) \tag{4}$$

$$\beta_{\text{Sn–O2}} = \beta_{ab} + \frac{1}{\sin\frac{\alpha_2}{2}}\left(\frac{d\sin\frac{\alpha_2}{2}}{dP}\right) \quad , \tag{5}$$

where $\beta_{ab} = \frac{(a^2+kb^2)\beta_a}{(a^2+b^2)}$ and $k = \beta_b/\beta_a$.The compressibilities of Sn–O bonds at room pressure can be calculated by using Eqs. (4) and (5), where *a*, *b*, *c* and α_i are substituted with the room-pressure values. From expressions (4) and (5), it is clear that compression of $R_{\text{Sn–O1}}$ is mainly controlled by compression of the *c* axis and variation of bending angle ∠Sn–O1–Sn. The average bond length compression $R_{\text{Sn-O2}}$ is determined by relative compression of *a* and *b* axis and variation in bending angle ∠ Sn–O2–Sn. If no octahedral tilting occurs, the equations suggest that the Sn–O bond compressibilities or octahedral compressibility are directly determined by the compressibilities of the three unit-cell axes. This, in turn, does not ensure that the CaO12 site is more compressible than the SnO6 site without octahedral tilting, even for k < 1 because $\beta_{ab}(k>1) > \beta_{ab}(k=1) > \beta_{ab}(k<1)$. Therefore, according to Eqs. (4) and (5), $d\sin(\alpha_i/2)/dP < 0$ is required for this trend to occur and this is the case observed at high pressure (Figs. 3 and 4).

According to Eqs. (4) and (5), by using $\alpha_i = 2\sin^{-1}[\exp(\Delta\beta_i P)\sin\alpha_{0i}/2]$, where α_{0i} is the room pressure value, the evolution of α_1 and α_2 with pressure can also be obtained from compressibility difference of $\Delta\beta_1(=\beta_{\text{Sn–O1}} - \beta_c)$ and $\Delta\beta_2(=\beta_{\text{Sn–O2}} - \beta_{ab})$, instead of from the refinements. The calculated angles from

Eqs. (4) and (5) would be more accurate because β_{Sn-O} and $\beta_{a,b,c}$ can be measured more accurately and $\Delta\beta$ might reduce possible systematic errors in measured $\beta_{Sn-O}$and $\beta_{a,b,c}$, as drawn (the hollow symbols) in Fig. 3a. This method would therefore be helpful to clarify small changes in the tilting that are otherwise obscured by the uncertainties of the measurement.

Conclusion

In summary, the evolution of the atomic-level structure of $CaSnO_3$ clearly involves the compression of both the CaO12 site and the SnO6 octahedron. Therefore a "rigid-unit" approach to the high-pressure behaviour of perovskites is inappropriate. Furthermore, the relative compressibility of the CaO12 and SnO6 sites plays an important role in the distortion of both sites with increasing pressure, as well as the change induced in the octahedral tilts. The compressibility of CaO12 site can be considered in two parts: the eight shorter bond lengths control the compression, whereas the changes in the four remaining longer distances are primarily related to the octahedral tilting, especially tilting associated with the Sn–O1–Sn angle. Therefore, for $CaSnO_3$ perovskite and those perovskites related to it, the differential compressibility of the AO8 and BO6 polyhedra determine the structural evolution of the perovskite with pressure.

Acknowledgments The authors acknowledge with gratitude the financial support for this work from NSF grant EAR-0105864. Ruby pressure measurements were conducted with the Raman system in the Vibrational Spectroscopy Laboratory in the Department of Geosciences at Virginia Tech with the help of Mr. Charles Farley.

References

Anderson DL, Anderson OL (1970) Bulk modulus–volume relationship for oxides. J Geophys Res 75: 3494–3500

Andrault D, Poirier JP (1991) Evolution of the distortion of perovskites under pressure: an EXAFS study of $BaZrO_3$, $SrZrO_3$ and $CaGeO_3$. Phys Chem Miner 18: 91–105

Angel RJ (2000) Equation of state. In: Hazen RM, Downs RT (eds) High-pressure, high-temperature crystal chemistry. Reviews in Mineralogy and Geochemistry, vol 41. Mineralogical Society of America, Washington, DC pp 35–59

Angel RJ (2003a) Automated profile analysis for single-crystal diffraction data. J Appl Crystallogr 36: 295–300

Angel RJ (2003b) Absorb software. www.crystal.vt.edu/crystal/software

Angel RJ, Downs RT, Finger LW (2000) High-temperature-high-pressure diffractometry. In: Hazen RM , Downs RT (eds) High-pressure, high-temperature crystal chemistry. Reviews in Mineralogy and Geochemistry Mineralogical Society of America, vol 41. Washington, DC pp 559–596

Angel RJ, Zhao J, Ross NL (2003) High quality at high pressure? Some further thoughts on single-crystal X-ray diffraction in the diamond cell. CMSEC conference, Study of matter at extreme conditions Miami, FA, 2003

Burnham CW (1966) Computation of absorption corrections and the significance of end effects. Am Mineral 51: 159–167

Dove MT (1997) Theory of displacive phase tranisitons in mineral. Am Mineral 82: 213–244

Dove MT, Heine V, Hammonds KD (1995) Rigid-unit modes in framework silicates. Mineral Mag 59: 629–639

Finger LW, King HE (1978) A revised method of operation of the single-crystal diamond cell and refinement of strucutre of NaCl at 32 kbar. Am Mineral 63: 337–342

Finger LW, Prince E (1975) A system of Fortran IV computer program for crystal strucutre computations. US Nat Bur Stand, NBS Tech note, 854, Washington, DC

Glazer AM (1972) The classification of tilted octahedra in perovskites. Acta Crystallogr B28: 3384–3392

Hammonds KD, Bosenick A, Dove MT, Heine V (1998) Rigid modes in crystal structures with octahedrally coordinated atoms. Am Min 83: 476–479.

Hazen RM, Finger LW (1982) Comparative crystal chemistry. Wiley New York, pp 231

King HE, Finger LW (1979) Diffraction beam crystal centering and its application to high pressure crystallography. J Appl Crystallogr 12: 374–378

Kung J, Angel RJ and Ross NL (2001) Elasticity of $CaSnO_3$ perovskite. Phys Chem Miner 28: 35–43

Lelieveld R, Ijdo D (1980) Sulphides with the $GdFeO_3$ structure. Acta Crystallogr B36: 2223–2226

Mao HK, Xu J, Bell PM (1986) Calibration of the ruby pressure gauge to 800kbar under quasi-hydrostatic conditions. J Geophys Res 91: 4673–4676

Miletich R, Allan DR, Kuhs WR (2000) High-pressure single-crystal techniques. In: Hazen RM, Downs RT (eds), High-pressure, high-temperature crystal chemistry, Reviews in Mineralogy and Geochemistry, vol 41. Mineralogical Society of America, Washington, DC, pp 445–520

Navrotsky A,Weidner D (1989) Perovskite, a structure of great interest to geophysics and materials science. American Geophysical Union Mon 45, Washington, DC

O'Keeffe M, Hyde B, Bovin J (1979) Contribution to the crystal chemistry of orthorhombic perovskites: $MgSiO_3$ and $NaMgF_3$. Phys Chem Miner 4: 299–305

Ross NL (1996) Distortion of $GeFeO_3$-type peroskites with pressure: a study of $YAlO_3$ to 5 GPa. Phase Trans 58: 27–41

Ross NL (1998) High pressure study of $ScAlO_3$ peroskite. Phys Chem Miner 25: 597–602

Ross NL, Chaplin TD (2003) Compressibility of $CaZrO_3$ perovskite: comparison with Ca-oxide perovskites. J Solid State Chem 172: 123–126

Ross NL, Hazen RM (1990) High-pressure crystal chemistry of $MgSiO_3$ perovskite. Phys Chem Miner 17: 228–237

Vegas A, Vallet-Regi M, Alario-Franco M (1986) The $ASNO_3$ (A = Ca, Sr) perovskites. Acta Crystallogr (B)42: 167–172

Woodward PM (1997a) Octahedral tilting in perovskites. I. Geometrical considerations. Acta Crystallogr B52: 32–43

Woodward PM (1997b) Octahedral tilting in perovskites. II. structure stabilizing forces. Act. Crystallogr B53: 44–66

Zhao Y, Weidner DJ, Parise JB, Cox DE (1993a) Critical phenomena and phase transition of perovskite—data for $NaMgF_3$ perovskite, part II. Phys Earth Planet Inter 76: 17–34

Zhao Y, Weidner DJ, Parise JB,Cox DE (1993b) Thermal expansion and structural distortion of perovskite—data for $NaMgF_3$ perovskite, part I. Phys Earth Planet Inter 76: 1–16